RSC Advances

ROYAL SOCIETY OF CHEMISTRY

www.rsc.org/advances

Journal Name

RSCPublishing

ARTICLE

Hydroxyapatite nanospheres supported ruthenium(0) nanoparticles catalyst for hydrogen generation from ammonia-borane solution: kinetic studies for nanoparticles formation and hydrogen evolution

Cite this: DOI: 10.1039/x0xx00000x

Received 00th January 2012,
Accepted 00th January 2012

DOI: 10.1039/x0xx00000x

www.rsc.org/

Halil Durak,[a] Mehmet Gulcan,[a] Mehmet Zahmakiran,[a*] Saim Ozkar,[b] Murat Kaya[c]

The development of readily prepared effective heterogeneous catalysts for the hydrogen generation from the ammonia-borane (AB; NH3BH3) solution under mild conditions remains a challenge in the field of "Hydrogen Economy". In this study, we report finding of an in-situ generated, highly active ruthenium nanocatalyst for dehydrogenation of ammonia-borane in water at room temperature. Our new catalyst system consisting of ruthenium(0) nanoparticles supported on nanohydroxyapatite (RuNPs@*nano*-HAp) and can reproducibly be prepared under in-situ conditions from the ammonia-borane reduction of a Ru^{3+} ions exchanged into nanohydroxyapatite (Ru^{3+}@*nano*-HAp) during the hydrolytic dehydrogenation of ammonia-borane at 25 ± 0.1 °C. Nanohydroxyapatite supported ruthenium(0) nanoparticles were characterized by using a combination of advanced analytical techniques. The sum of their results shows the formation of well-dispersed ruthenium(0) nanoparticles with a mean diameter of 2.6 ± 0.6 nm, on the surface of nanospheres of hydroxyapatite by keeping the host matrix intact. The resulting RuNPs@*nano*-HAp are highly active catalyst in the hydrolytic dehydrogenation of ammonia-borane with an initial TOF value of 205 min^{-1} by generating 3.0 equiv. of H2 per mole of ammonia-borane at 25 ± 0.1 °C. Moreover, they are stable enough to be isolated and bottled as solid materials, which can be reused as active catalyst under the identical conditions of the first run. The work reported here also includes the following results; *(i)* Monitoring the formation kinetics of the in-situ generated RuNPs@*nano*-HAp by using the hydrogen generation from the hydrolytic dehydrogenation of ammonia-borane as reporter reaction. The sigmoidal kinetics of catalyst formation and concomitant dehydrogenation fits well to the two-step, slow nucleation and then autocatalytic surface growth mechanism, P→Q (rate constant k_1) and P+Q→2Q (rate constant k_2), in which P is Ru^{3+}@*nano*-HAp and Q is the growing, catalytically active RuNPs@*nano*-HAp, *(ii)* The compilation of kinetic data for the RuNPs@*nano*-HAp catalyzed hydrolytic dehydrogenation of ammonia-borane depending on the temperature and catalyst concentration to determine the dependency of reaction rate on the catalyst concentration and the activation parameters (Ea, $\Delta H^{\#}$, and $\Delta S^{\#}$) of the reaction.

Introduction

Nowadays, the development of safe and efficient hydrogen storage technologies is one of the most important and challenging problems in the hydrogen based energy policies,[1,2] which would make possible the changeover from fossil fuels to the renewable energy sources.[3,4] For this reason, a numerous studies have been performed for the development of materials with high volumetric and gravimetric storage capacity, as the low density of hydrogen makes it difficult to store in compressed or liquefied form.[3] In this context, various porous materials[5-8] boron based chemical hydrides[9-11] and boron-nitrogen compounds[12-16] have been tested for chemical hydrogen storage. Among these materials, ammonia-borane

(AB; NH_3BH_3) has been found to be much better suited for this purpose due to the following advantages (*i*) AB has high gravimetric hydrogen storage capacity (19.6 % wt), (*ii*) it has low molecular weight (30.7 $g.mol^{-1}$), (*iii*) it is non-flammable and non-explosive under standard conditions.[17] These significant properties make AB unique compared to metal hydrides/B-N compounds or porous materials, where the hydrogen release and uptake can be controlled by temperature and pressure. Although hydrogen can be released from AB through its' thermal decomposition,[18] dehydrocoupling,[19] and alcoholysis,[20] there is much interest in the transition metal catalyzed hydrolytic dehydrogenation[12] due to favorable kinetics and mild reaction conditions. The hydrolytic dehydrogenation of AB generates 3 equiv. of H_2 (per mole of AB) at room temperature (RT) under air only in the presence of a suitable catalyst (**1**).[12,17,21,22]

$$NH_3BH_3 + 3H_2O \xrightarrow[\text{at RT under air}]{\text{catalyst}} NH_4BO_2 + 3H_2 \quad (1)$$

Despite the difficulty in recycling of the hydrolysis product metaborate anion, the hydrogen generation from the hydrolytic dehydrogenation of ammonia-borane has several features, which make it promising for potential applications; (*i*) AB has high solubility in water (33.6 g/100 g H_2O),[23] (*ii*) the reaction takes place at appreciable rate only in the presence of a suitable catalyst at room temperature, (*iii*) the hydrolytic dehydrogenation of AB is exothermic (ΔH = -155.97 kJ/mol).[24] Many transition metals or their compounds have been tested as catalyst in hydrogen generation from the hydrolysis of AB.[25] Of particular importance are the, ruthenium based heterogeneous catalyst showing high activity in the hydrolytic dehydrogenation of AB under mild conditions.[26-33] Unfortunately, most of them used in these schemes suffer from difficult isolation,[28,31,32] low activity[29,30,33] low stability,[31,32] and time consuming synthesis procedures.[27,28,32] Therefore, the development of readily accessible, highly active and reusable catalyst that operates under mild conditions remains a challenge in the field.

Recently, hydroxyapatite ($[Ca_{10}(OH)_2(PO_4)_6]$, HAp)[34] has generated great interest in view of its potential usefulness as a catalyst support with attractive properties.[35,36,37] Particularly, HAp has the following advantages as a catalyst support: (*i*) reduced mass transfer limitations due to the absence of structural porosity, (*ii*) a high ion-exchange and adsorption capacity, and (*iii*) low surface acidity that prevent side reactions arising from the support itself.[6] These physicochemical properties of HAp prompted us to focus on the use of the HAp matrix in the stabilization of metal nanoparticles. We have recently reported that ruthenium(0) nanoparticles supported on the surface of HAp are highly active, long lived and reusable catalyst providing 87,000 turnovers with an initial turnover frequency value of 137 min^{-1} in hydrogen generation from the hydrolysis of AB at 25.0 ± 0.1 °C.[38] Additionally, we have also shown that the reduction of the particle size of support materials from the *micro*-size to *nano*-size regime (from >1 μm to <100 nm) results in a tremendous increase of external surface area, a larger number of exchange sites and lower mass transfer limitations for the catalytic applications.[37,39]

Herein we report the use of colloidal hydroxyapatite nanospheres with particle size smaller than 50 nm as support in the stabilization of ruthenium(0) nanoparticles. Ruthenium(0) nanoparticles supported on the surface of *nano*-HAp , hereafter referred to as RuNPs@*nano*-HAp, show remarkable catalytic performance in terms of activity and reusability in the hydrolytic dehydrogenation of AB at room temperature under air. RuNPs@*nano*-HAp can reproducibly be prepared by the ion exchange of Ru^{3+} ions with Ca^{2+} ions of the *nano*-HAp matrix, followed by the *in-situ* AB reduction of Ru^{3+} ions on the surface of colloidal HAp during the hydrolytic dehydrogenation of AB. After a short induction time period, the resulting RuNPs@*nano*-HAp catalyzes the dehydrogenation of aqueous AB solution at room temperature with an *initial* turnover frequency (TOF) of 205 min^{-1}. More importantly, *nano*-HAp dispersed ruthenium(0) nanoparticles feature notable resistance against agglomeration and leaching throughout the catalytic runs. Indeed, when the isolated RuNPs@*nano*-HAp are reused, they retain 92 % of their initial catalytic activity even at 5th reuse in the hydrolytic dehydrogenation of AB.

Experimental

Materials

Synthetic hydroxyapatite nanocrystalline powder ($[Ca_5(OH)(PO_4)_3]_x$, ≥99.995% trace metals basis), ruthenium(III) chloride trihydrate ($RuCl_3.3H_2O$), ammonia-borane (NH_3BH_3, 97 %), D_2O and $BF_3{\cdot}(C_2H_5)_2O$ were purchased from Sigma-Aldrich. Deionized water was distilled with a water purification system (Thermo Scientific Barnsted Nanopure System). All glassware and Teflon-coated magnetic stir bars were cleaned with acetone, followed by copious rinsing with doubly deionized water under ultrasonication, and finally dried in an oven at 423 K.

Characterization

XRD data for *nano*-HAp, Ru^{3+}@*nano*-HAp and RuNPs@*nano*-HAp were collected using Rigaku X-ray Diffractometer (Model, Miniflex) with Cu-Kα (30 kV, 15 mA, =1.54051 Å) radiation at room temperature. TEM samples were prepared by dropping one drop of dilute suspension on copper coated carbon TEM grid and the solvent was then evaporated at room temperature under reduced pressure (10^{-3} torr). The conventional TEM was carried out on a JEOL JEM-200CX transmission electron microscopes operating at 120 kV. The ruthenium content of RuNPs@*nano*-HAp was determined by inductively coupled plasma atomic emission spectroscopy (ICP-OES; ULTIMA 2-HORIBA Jobin-Yvon) after the powdered sample was completely dissolved in the mixture of HNO_3:HCl with a 1:3 ratio. The nitrogen adsorption/desorption experiments were carried out at 77 K using a NOVA 3000 series (Quantachrome Inst.) instrument. The sample was outgassed under vacuum at 393 K for 3 h before the adsorption of nitrogen. XPS analysis was performed on a Kratos AXIS

ultra imaging X-ray photoelectron spectrometer using monochromatic Al Kα radiation (1486.6 eV, the X-ray tube working at 15 kV, 350 W and pass energy of 23.5 keV). At the end of the hydrolysis reaction, the resulting solutions were filtered and the filtrates were collected for ^{11}B NMR analysis. ^{11}B NMR spectra were recorded on a Bruker Avance DPX 400 with an operating frequency of 128.15 MHz. D_2O and $BF_3{\cdot}(C_2H_5)_2O$ were used as a lock and an external reference, respectively.

Preparation of ruthenium(III)-exchanged nanohydroxyapatite (Ru^{3+}@*nano*-HAp) precatalyst and the general procedure for the *in-situ* generation of ruthenium(0) nanoparticles supported on nanohydroxyapatite (RuNPs@*nano*-HAp)

Ruthenium(III) cations were introduced into Ca^{2+}@*nano*-HAp by the ion exchange of 200 mg of Ca^{2+}@*nano*-HAp in 10 mL of an aqueous solution of 5.23 mg of $RuCl_3{\cdot}3H_2O$ (0.02 mmol) for 12 h at room temperature. The sample was then filtered by suction filtration using a Whatman-1 filter (Ø = 9 cm), washed three times with 100 mL of deionized water, and dried at 353 K in the oven. The *in-situ* formation of RuNPs@*nano*-HAp and the concomitant hydrolytic dehydrogenation of AB were performed in a Fischer−Porter (F−P) pressure bottle connected to a line through Swagelock tetrafluoroethylene (TFE)-sealed quick connects and to an Omega-PX209-100GI pressure transducer interfaced through an Omega-UWPC-2-NEMA wireless transmitter to a computer using an Omega-UWTC-REC2-DV2 wireless receiver. The progress of an individual dehydrogenation reaction was followed by monitoring the pressure of H_2 gas on the Omega-data logging and using the recording software program. In a typical experiment, 100 mg of Ru^{3+}@*nano*-HAp (4.16 μmol Ru) was weighted and placed in a new 22 × 175 mm pyrex culture tube containing a new 5/16 in. × 5/8 in. stir bar. The culture tube was then placed inside the F−P bottle, and the entire setup was placed inside a constant-temperature circulating water bath thermostatted at 25 ± 0.1 °C. Next, 10.0 mL of 100 mM AB solution was added to the F−P bottle rapidly via a syringe with a long needle and the reaction timer was started (t = 0 min). When no more hydrogen generation was observed, the experiment was stopped, the F−P bottle was closed and disconnected from the line, and the hydrogen pressure was released. Finally, a small aliquot from the reaction solution in the culture tube was withdrawn for ^{11}B NMR analysis.

Data handling and curve fit for the hydrogen generation data.

The raw pressure versus time data collected with the computer-interfaced transducer were exported from Omega software program and imported into OriginPro 8, which was then converted into the volume of hydrogen (mL). The curve fitting of equivalent H_2 generated per NH_3BH_3 versus time data to the Finke−Watzky two-step mechanism[40,41] was performed as described elsewhere[40,41,42] using the software package OriginPro 8, which is a nonlinear regression subroutine and uses a modified Levenberg−Marquardt algorithm.[43]

Isolability and reusability of RuNPs@*nano*-HAp in the hydrolytic dehydrogenation of ammonia-borane

After the first run of the hydrolytic dehydrogenation of 100 mM AB in 10 mL H_2O catalyzed by 100 mg RuNPs@*nano*-HAp (4.16 μmol Ru) at 25 ± 0.1 °C, the catalyst was isolated by suction filtration, washed three times with 20 mL of deionized water, and dried under N_2 gas purging at room temperature then transferred into the glove box. The dried samples of RuNPs@*nano*-HAp were weighted and used again in the hydrolytic dehydrogenation of 100 mM AB in 10 mL H_2O and the same procedure was repeated up to 5th catalytic cycle. The results were expressed as percentage of the retained *initial* catalytic activity of RuNPs@*nano*-HAp in the hydrolytic dehydrogenation of AB versus number of catalytic runs.

Results and Discussion

***In-situ* formation of RuNPs@*nano*-HAp during the hydrolytic dehydrogenation of AB starting with Ru^{3+}@*nano*-HAp precatalyst and the characterization of the resulting RuNPs@*nano*-HAp**

Ruthenium(0) nanoparticles supported on nano-hydroxyapatite, referred to as RuNPs@*nano*-HAp, can reproducibly be prepared by the ion-exchange[44] of Ru^{3+} ions with Ca^{2+} ions of the HAp matrix followed by AB reduction of the resulting Ru^{3+}@*nano*-HAp precatalyst during the hydrolytic dehydrogenation of AB. The progress of nanoparticles formation and associated hydrolytic dehydrogenation of AB was followed by monitoring the changes in hydrogen pressure, which was then converted into the equivalent H_2 generated per mole of AB, using the known 3:1 H_2/AB stoichiometry (**1**). Fig. 1 shows the plot of equivalent hydrogen generated per mole of AB versus time for the hydrolytic dehydrogenation of AB starting with Ru^{3+}@*nano*-HAp precatalyst at 25 ± 0.1 °C. The formation kinetics of RuNPs@*nano*-HAp catalyst can be obtained by using the hydrolysis of AB as reporter reaction,[40,45,46] (*Scheme 1*), in which A is the added precatalyst Ru^{3+}@*nano*-HAp and B is the growing RuNPs@*nano*-HAp catalyst. The hydrolytic dehydrogenation of AB will truthfully report and intensify the amount of RuNPs@*nano*-HAp catalyst, Q, present if the hydrolysis rate is fast in comparison to the rate of nanoparticles formation.

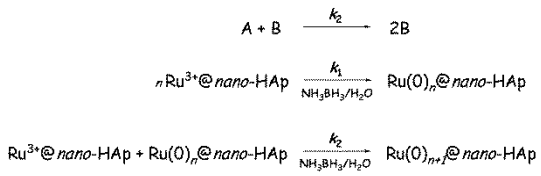

Scheme 1. Minimalistic, two-step nanoparticles nucleation then autocatalytic surface growth mechanism[40] for *in-situ* generated RuNPs@*nano*-HAp during the hydrolytic dehydrogenation of AB.

The sigmoidal kinetic can be seen in Fig. 1, just as an example of all of the data collected under different conditions (*vide infra*), and fits well by the Finke-Watzky two-step nucleation and autocatalytic growth mechanism of nanoparticles formation.[40] The observation of a sigmoidal dehydrogenation curve and its curve fit to the slow, continuous nucleation A→B (rate constant k_1) followed by autocatalytic surface growth A+B→2B (rate constant k_2) kinetics is indicative of the formation of a metal(0) nanoparticles catalyst from a precatalyst in the presence of a reducing agent.[40,41,42] The rate constants determined from the nonlinear least-squares curve fit from Fig. 1 are $k_1 = 3.27\times10^{-2}$ min^{-1} and $k_2 = 14.65$ M^{-1}. min^{-1} (the k_2 has been corrected to the stoichiometry factor of 400, as described elsewhere).[45]

After the generation of 3 equiv. of H_2 plus judgment of AB (δ = -23 ppm, q) conversion to metaborate (δ = 9 ppm, s) by ^{11}B NMR spectroscopy,[47] the resulting RuNPs@*nano*-HAp were isolated by filtration and characterized by using several analytical techniques. Fig. 2 depicts the XRD patterns of *nano*-HAp, Ru^{3+}@*nano*-HAp and RuNPs@*nano*-HAp (with 0.51 % wt. Ru loading as determined by ICP-OES) altogether and the comparison of them clearly shows that the incorporation of ruthenium(III) ions into *nano*-HAp and the reduction of ruthenium(III) ions forming the ruthenium(0) nanoparticles on the surface of *nano*-HAp cause no observable alteration in the framework lattice and no loss in the crystallinity of *nano*-HAp. The morphology and the size of RuNPs@*nano*-HAp were investigated by using transmission electron microscopy (TEM). TEM images of RuNPs@*nano*-HAp in different magnifications given in Fig. 3 reveal the existence of ruthenium(0) nanoparticles with an average diameter of 2.6 ± 0.6 nm (Fig. 3(d)), which corresponds to $Ru(0)_{\sim650}$ nanoclusters,[48] on the surface of HAp-*nanospheres* of 60-80 nm size. N_2 adsorption–desorption isotherms of *nano*-HAp and RuNPs@*nano*-HAp (0.51 wt% Ru loading) are given in Fig. 4.

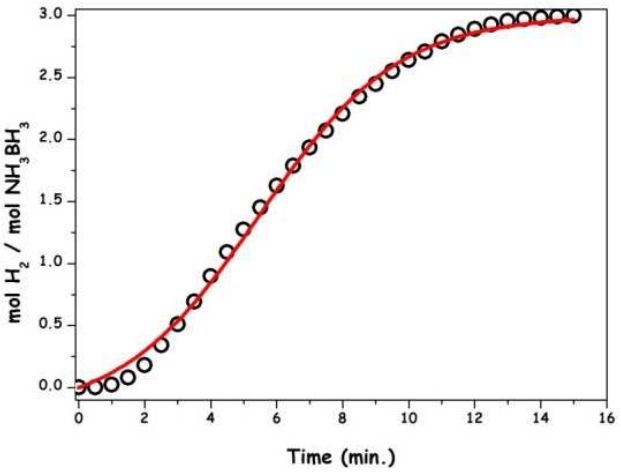

Fig. 1. Plot of generation of equivalent H_2 per NH_3BH_3 versus time (min.) for the *in-situ* generated RuNPs@*nano*-HAp catalyzed hydrolytic dehydrogenation of AB starting with Ru^{3+}@*nano*-HAp precatalyst ([AB] = 100 mM; [Ru] = 0.25 mM in 10.0 mL H_2O) at 25 ± 0.1 ºC and its curve fit (red) to F–W two-step nucleation and autocatalytic growth mechanism[40] (k_1 = (3.27 ± 0.19) ×10^{-2} min^{-1}, k_2 = (14.65 ± 0.47) M^{-1}. min^{-1} and R^2 = 0.997) for ruthenium(0) nanoparticles formation.

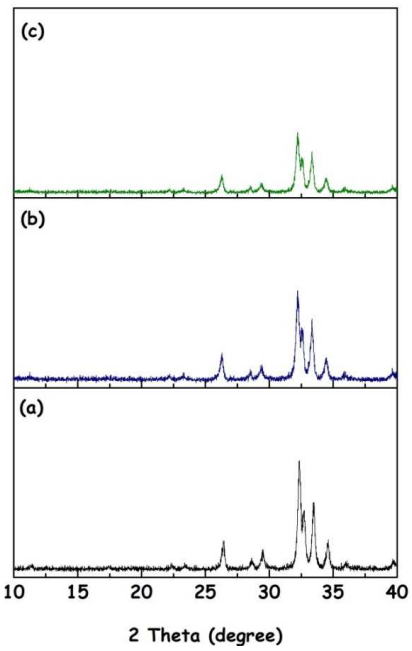

Fig. 2. The powder X-ray diffraction (P-XRD) patterns of (a) nano-HAp, (b) Ru3+@nano-HAp precatalyst, (c) RuNPs@nano-HAp.

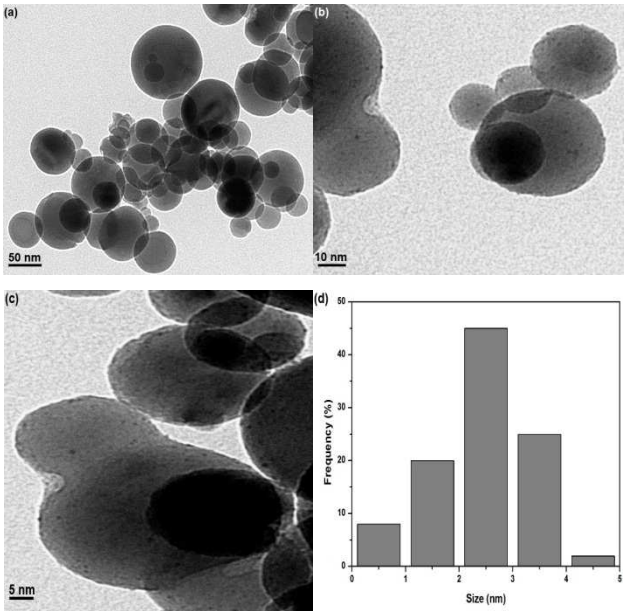

Fig. 3. (a-c) are TEM images in different magnifications, (d) corresponding size histogram of RuNPs@*nano*-HAp.

Both isotherms show Type III shape, reflecting the absence of micropores (< 2 nm).[49] On passing from *nano*-HAp to RuNPs@*nano*-HAp, the surface area is reduced from 40 to 28 m^2/g. The decrease in the surface area is associated with the presence of ruthenium nanoparticles on the *nano*-HAp surface. Furthermore, no hysteresis loop was observed in the N_2 adsorption-desorption isotherm of RuNPs@*nano*-HAp, indicating that the procedure followed in the preparation of RuNPs@*nano*-HAp does not create any mesopores within the framework of *nano*-HAp. The oxidation state of ruthenium in

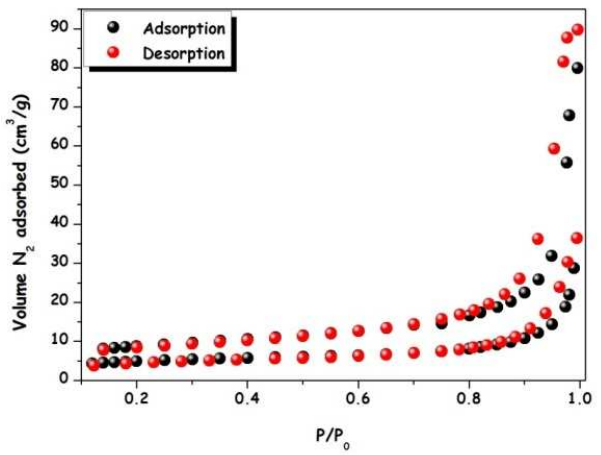

Fig. 4. Nitrogen-adsorption-desorption isotherms of nano-HAp (up) and RuNPs@nano-HAp (down).

the RuNPs@*nano*-HAp sample was investigated by X-ray photoelectron spectroscopy (XPS). Fig. 5 shows the high resolution Ru 3d and 3p XPS spectra of RuNPs@*nano*-HAp, which gives three prominent peaks at 287.2, 284.7, and 465.9 eV, readily assigned to Ru(0) $3d_{3/2}$, Ru(0) $3d_{5/2}$, and Ru(0) $3p_{3/2}$, respectively,[50] thus indicating the complete reduction of Ru^{3+} species *in-situ* during the hydrolytic dehydrogenation of AB. Compared to the value of metallic ruthenium 3d and 3p peaks, the slight shift (ΔE_b = 0.4 eV -0.6 eV) observed in RuNPs@*nano*-HAp toward a higher energy value can be attributed to the peculiar electronic properties of the HAp matrix.[35]

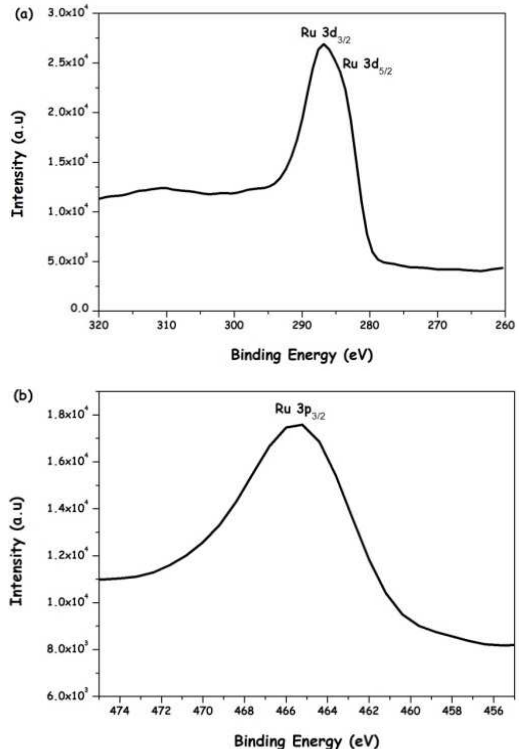

Fig. 5. High resolution (a) Ru 3d and (b) Ru 3p XPS spectra of RuNPs@*nano*-HAp.

Control experiments: (*i*) catalytic reactivity of the host material (*nano*-HAp) in the hydrolytic dehydrogenation of AB and (*ii*) effect of ruthenium loading on the catalytic activity of RuNPs@*nano*-HAp in the hydrolytic dehydrogenation of AB.

Before testing the catalytic activity of the in-situ generated RuNPs@*nano*-HAp in hydrogen generation from the hydrolysis of ammonia-borane, one has to check whether sole *nano*-HAp can catalyze the same reaction under the identical conditions. In the control experiments starting with sole nano-HAp, no hydrogen generation was observed from the hydrolysis of AB at 20, 25, 30, 35 and 40 °C in the same time intervals as the ones used for the RuNPs@*nano*-HAp catalyzed hydrolytic dehydrogenation of AB (vide infra). As the next, the hydrolytic dehydrogenation of AB was performed starting with Ru^{3+}@*nano*-HAp precatalyst with different ruthenium loadings in the range of 0.32 – 4.20 wt % to determine the effect of ruthenium loading on the catalytic activity of RuNPs@*nano*-HAp. Fig. 6(a) shows the plots of equivalent hydrogen generated per mole of AB versus time for the hydrolysis of AB starting with Ru^{3+}@*nano*-HAp precatalyst at 25 ± 0.1 °C with different metal loading.

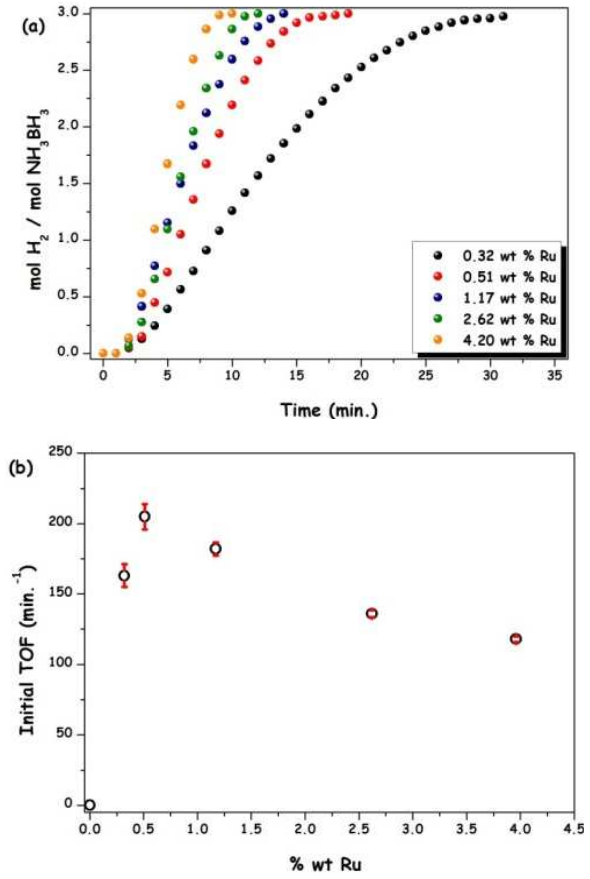

Fig. 6. (a) Plot of generation of equivalent H_2 per NH_3BH_3 versus time (min.) for the *in-situ* generated RuNPs@*nano*-HAp catalyzed hydrolytic dehydrogenation of AB starting with Ru^{3+}@*nano*-HAp precatalysts with Ru loadings of 0.32, 0.51, 1.17, 2.62 and 4.20 wt % (in all [AB] = 100 mM and 100 mg Ru^{3+}@*nano*-HAp precatalyst in 10.0 mL H_2O) at 25 ± 0.1 ºC, (b) Plot of initial TOF values versus Ru loadings (wt %).

The variation in the catalytic activity with the ruthenium loading given in Fig. 6, reflects the relative number of accessible ruthenium(0) atoms on the surface of nanoparticles supported on the *nano*–HAp spheres. The fraction of accessible ruthenium(0) atoms depends on the interaction between the host surface and nanoparticles plus the size of nanoparticles. The highest catalytic activity is obtained by using Ru^{3+}@*nano*-HAp precatalyst containing 0.51 wt % Ru, Indeed an informative TEM image taken from RuNPs@*nano*-HAp sample with 4.20 wt % Ru loading indicates the existence of larger ruthenium(0) nanoparticles (3.6 ± 0.9 nm) than that of the sample with 0.51 wt% Ru loading.

Determination of activation parameters (Ea, $\Delta H^{\#}$, $\Delta S^{\#}$) and rate dependency on [Ru] for the hydrolysis of AB catalyzed by the *in-situ* generated RuNPs@*nano*-HAp.

We determined the activation energy and activation parameters (Ea, $\Delta H^{\#}$ and $\Delta S^{\#}$) for the hydrolytic dehydrogenation of AB catalyzed by the *in-situ* generated RuNPs@*nano*-HAp from the temperature dependent kinetic data shown in Fig. 7. The observed rate constants were calculated from the nearly linear portions of the curves at different temperatures (Table 1) and used for the construction of Arrhenius and Eyring-Polonyi plots given in Figs. 8a and 8b, respectively: the activation energy, Ea = 55 ± 2 kJ/mol; activation enthalpy $\Delta H^{\#}$ = 51 ± 2 kJ/mol and activation entropy $\Delta S^{\#}$ = -51 ± 5 J/mol.K for the hydrolysis of AB catalyzed by the *in-situ* generated RuNPs@*nano*-HAp. The activation energy value is comparable with the majority of the previously employed Ru-based catalysts (*vide infra*). The small value of the activation enthalpy and the large negative value of the activation entropy imply an associative mechanism in the transition state for the hydrolytic dehydrogenation of AB catalyzed by the *in-situ* formed RuNPs@*nano*-HAp. The rate constants k_1 and k_2 obtained from the curve fit of the data to the two-step mechanism and the k_2/k_1 ratios are given in Table 1

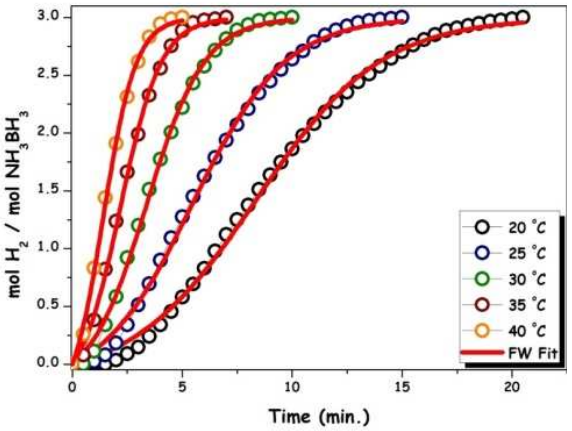

Fig. 7. Plot of generation of equivalent H_2 per NH_3BH_3 versus time (min.) and its curve fit (red) to F–W two-step nucleation and autocatalytic growth mechanism[40] for the *in-situ* generated RuNPs@*nano*-HAp catalyzed hydrolytic dehydrogenation of AB starting with Ru^{3+}@*nano*-Hap (0.51 wt % Ru) precatalyst at different temperatures (in all [AB] = 100 mM; [Ru] = 0.25 mM in 10.0 mL H_2O).

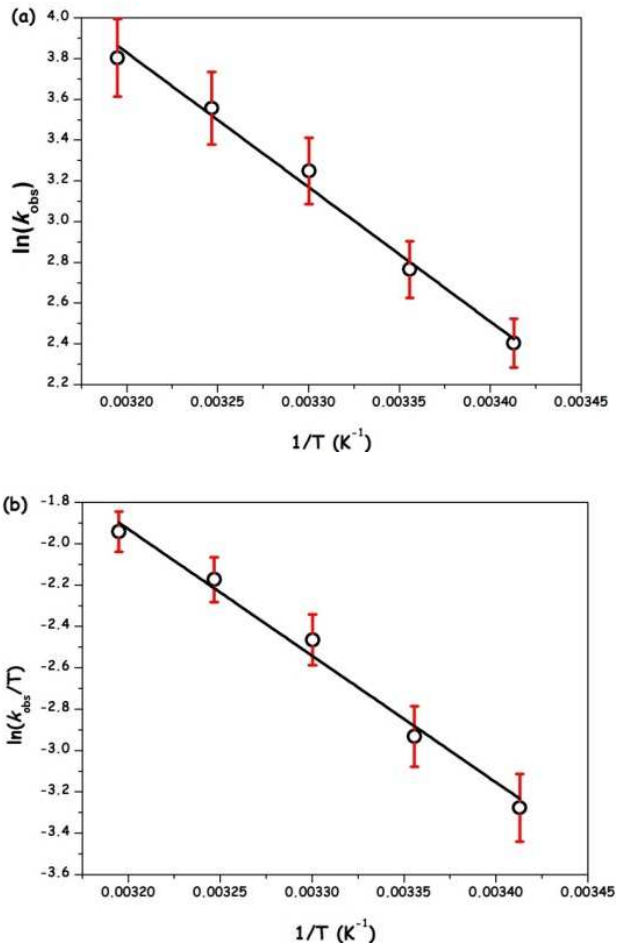

Fig. 8. (a) Arrhenius plot (y = 24.948 - 6599 x and R^2 = 0.988) and (b) Eyring-Polanyi plot (y = 17.665 - 6122 x and R^2 = 0.981) for the *in-situ* generated RuNPs@nano-HAp catalyzed hydrolytic dehydrogenation of AB starting with Ru^{3+}@*nano*-HAp precatalyst.

together with the induction time periods and the hydrogen generation rates obtained from the nearly linear portions of the curves for the hydrolysis of AB at different temperatures. While the induction period decreases, the k_1 and k_2 rate constants increase with the increasing temperature expectedly. The inverse relationship between the induction time and the rate constant k_1, which has been known for a long time[40] is also observed in our case. Another important point that can be concluded from the inspection of the data listed in Table 1, is the large values of k_2/k_1 ratio, which implies the high level of kinetic control for the formation of ruthenium(0) nanoparticles supported on *nano*-HAp.The kinetics of hydrolytic dehydrogenation of AB catalyzed by RuNPs@*nano*-HAp was also studied depending on the catalyst concentration to establish the rate law for the catalytic transformation. Fig. 9a shows the plots of equivalent H_2 generated per mole of AB versus time during the hydrolytic dehydrogenation of AB starting with Ru^{3+}@*nano*-HAp precatalyst (0.51 wt % Ru) in different ruthenium concentrations at 25.0 ± 0.1 ºC. A fast dehydrogenation starts after an induction time of 4.0 – 0.3 min.

Table 1. k_1, k_2, t (induction time), k_2/k_1 and k_{obs} (dehydrogenation rate) of *in-situ* generated RuNPs@*nano*-HAp catalyzed hydrolytic dehydrogenation of AB ([AB] = 100 mM; [Ru] = 0.25 mM in 10.0 mL H_2O) depending on temperature.

entry	T (°C)	k_1 (min^{-1}) $\times 10^2$	k_2 $(M.min)^{-1}$	k_2/k_1 (M^{-1}) $\times 10^2$	t (min.)	k_{obs} (mM/min)
1	20	1.75 ± 0.09	44.77 ± 1.09	25.58 ± 1.95	1.50	11.06
2	25	3.27 ± 0.19	59.21 ± 1.89	18.10 ± 1.62	0.83	15.88
3	30	5.35 ± 0.35	94.61 ± 3.47	17.68 ± 1.81	0.58	25.77
4	35	9.29 ± 0.66	131.59 ± 5.73	14.17 ± 1.62	0.33	35.04
5	40	17.41 ± 1.31	157.73 ± 9.01	9.06 ± 1.19	0.17	44.87

The dehydrogenation rate, determined from the nearly linear portion of the plots, increases with the catalyst concentration (Table 2). Plotting the hydrogen generation rate versus ruthenium concentration, both on logarithmic scales, gives a straight line with a slope of 0.92 (Fig. 9b). That is, an apparent first-order dependence on the catalyst concentration is observed. As seen from Fig. 9a, the experimental data in all ruthenium concentrations fit well to the Finke-Watzky two-step nanoparticle formation mechanism,[40] which provides the rate constants k_1 of the slow, continuous nucleation, P → Q, and k_2 of the autocatalytic surface growth, P + Q → 2Q (Table 2). Expectedly, nucleation rate constant k_1 for the nucleation increases with the increasing [AB]/[Ru] ratio, and the rate constant k_2 for surface growth decreases with the increasing ruthenium concentration. More importantly, the k_2/k_1 ratio decreases with the increasing ruthenium concentration, indicating that the nanoparticle formation becomes less kinetically controlled in more concentrated solution.

Apart from activity, the reusability of RuNPs@*nano*-HAp, as another crucial measure in heterogeneous catalysis, was also examined in the hydrolysis of AB. When isolated and dried sample of RuNPs@*nano*-HAp catalyst is reused in AB hydrolysis, RuNPs@*nano*-HAp are still acting as active catalyst, they retain almost their inherent catalytic activity (> 94 %) even at complete conversion (≥ 99 %).

The effect of the size of host HAp matrix on the catalytic activity of guest ruthenium(0) nanoparticles "activity comparison of RuNPs@*nano*-HAp with RuNPs@*micro*-HAp".

We have recently reported[38] the activity of ruthenium(0) nanoparticles supported on *micro*-sized HAp (≥ 1 μm) in hydrogen generation from the hydrolysis of AB at 25.0 ± 0.1 °C. Since both catalysts were prepared in the same way by using the same support but in different particles sizes, we can make a comparison for the size effect of the support materials on the catalytic activity of guest ruthenium(0) nanoparticles. The ruthenium(0) nanoparticles supported on *nano*-HAp show

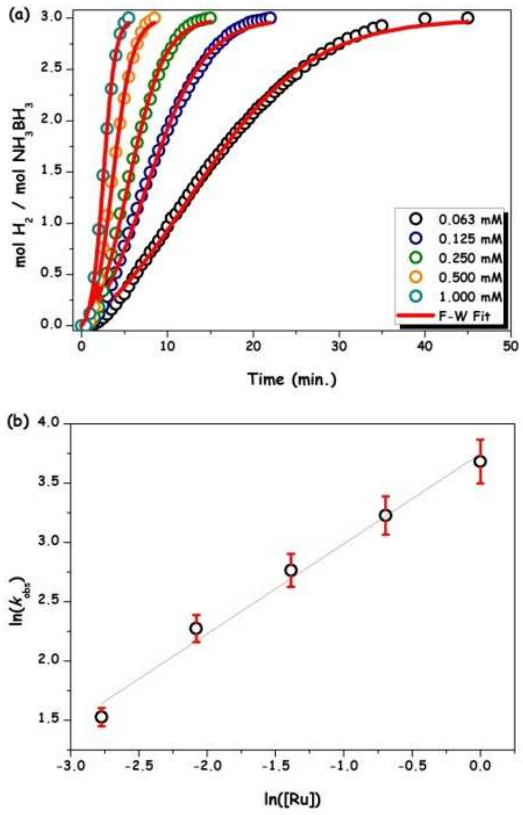

Fig. 9. (a) Plot of generation of equivalent H_2 per NH_3BH_3 versus time (min.) its curve fit (red) to F–W two-step nucleation and autocatalytic growth mechanism[40] for the hydrolytic dehydrogenation of AB starting with Ru^{3+}@*nano*-HAp precatalyst (in all [AB] = 100 mM in 10.0 mL H_2O) at different ruthenium concentrations as given on the graph at 25 ± 0.1 ºC, (b) ln(k_{obs}) versus ln([Ru]) graph ($y = 3.748 - 0.919\,x$ and $R^2 = 0.998$).

an activity of TOF = 205 min^{-1} in hydrogen generation from the hydrolysis of AB at 25.0 ± 0.1 °C while the ruthenium(0) nanoparticles supported on the micro-HAp show an activity of TOF = 137 min^{-1} in the same reaction. This notable difference in the activity of ruthenium(0) nanoparticles supported on hydroxyapatite in nano and micro can be attributed to the larger surface area of *nano*-HAp spheres than the micro-HAp particles and to the smaller size of the ruthenium(0) nanoparticles supported on the *nano*-HAp (2.56 ± 0.61 nm) than that of nanoparticles supported on the *micro*-HAp particles (4.70 ± 0.70 nm). Both of these phenomena are the consequences of the reduction of the particle size of HAp matrix from the *micro*-size to *nano*-size regime (from >1 μm to <100 nm).

Conclusions

In summary, our study on the preparation and characterization of ruthenium(0) nanoparticles supportes on the surface of hydroxyapatite nanospheres as well as their catalytic use in hydrogen generation from the hydrolysis of ammonia-borane plus the detailed kinetics of both nanoparticles formation and hydrogen evolution has led to the following conclusions and insights:

Table 2. k_1, k_2, k_2/k_1 and k_{obs} (dehydrogenation rate) of the *in-situ* generated RuNPs@*nano*-HAp catalyzed hydrolytic dehydrogenation of AB at 25 ± 0.1 ºC depending on [Ru] concentrations.

entry	[AB] (mM)	[Ru] (mM)	k_1 (min^{-1}) $\times 10^2$	k_2 $(M.min)^{-1}$	k_2/k_1 (M^{-1}) $\times 10^{-2}$	k_{obs} (mM/ min)
1	100	0.063	2.02 ±0.06	65.28 ±1.53	32.30 ±1.60	4.60
2	100	0.125	2.88 ±0.12	71.12 ±1.90	24.70 ±1.70	9.72
3	100	0.250	3.27 ±0.19	59.21 ±1.89	18.10 ±1.62	15.88
4	100	0.500	3.48 ±0.32	55.76 ±2.21	16.02 ±2.11	25.22
5	100	1.000	3.59 ±0.46	46.70 ± 2.16	13.01 ±0.23	39.72

(*i*) For the first time, nanohydroxyapatite supported ruthenium(0) nanoparticles, RuNPs@*nano*-HAp, were reproducibly prepared from the *in-situ* reduction Ru^{3+}@*nano*-HAp during the hydrolytic dehydrogenation of ammonia-borane at room temperature,

(*ii*) The characterization of the resulting novel catalytic material by using ICP-OES, XRD, XPS, TEM and N_2-adsorption-desorption techniques reveals that the formation of well-dispersed $Ru(0)_{\sim 650}$ nanoparticles (2.56 ± 0.61 nm) on the surface of hydroxyapatite *nanospheres* by keeping the host matrix intact;

(*iii*) Ruthenium(0) nanoparticles supported on *nano*-hydroxyapatite show notable catalytic activity (lower-bound TOF_{inital} = 205 min^{-1}) among all the heterogeneous ruthenium catalysts tested in the hydrolytic dehydrogenation of AB at room temperature,

(*iv*) Ruthenium(0) nanoparticles show high stability against the sintering and leaching, which make them highly reusable catalyst; when redispersed they retain almost their initial activity even at the 5th catalytic run in the hydrolytic dehydrogenation of ammonia-borane releasing 3 equiv. of H_2 per mole of ammonia-borane,

(*v*) The quantitative kinetic studies depending on the catalyst concentration and temperature reveal that the hydrolytic dehydrogenation of ammonia-borane catalyzed by ruthenium(0) nanoparticles is first-order in catalyst concentration. The activation parameters were also determined for the hydrolytic dehydrogenation of ammonia-borane catalyzed by ruthenium(0) nanoparticles supported on nano-hydroxyapatite. The small values of the activation energy and enthalpy (Ea = 55 kJ/mol, $\Delta H^{\#}$ = 51 kJ/mol) and the negative value of the activation entropy ($\Delta S^{\#}$ = -51. J/mol.K) are indicative of an associative mechanism in the transition state for the catalytic hydrolysis of ammonia-borane,

(*vi*) All of the kinetic data, collected for the formation of ruthenium(0) nanoparticles and concomitant hydrolytic dehydrogenation of ammonia-borane under various experimental conditions, fit well to the two-step mechanism for the nanoparticles formation:[40] continuous nucleation A→ B (rate constant k_1) followed by autocatalytic surface growth A+B→2B (rate constant k_2). The large values of the k_2/k_1 ratio obtained at different conditions are indicative of the high level of kinetic control in the formation of ruthenium(0) nanoparticles from the reduction of ruthenium(III) ions exchanged to the *nano*-hydroxyapatite,

(*vii*) The reporter reaction method developed by Finke *et al.*[51] for the catalytic hydrogenation of olefins and aromatics was shown to work also in the case of ruthenium(0) nanoparticles formation from the reduction of ruthenium(III) ions exchanged to *nano*-hydroxyapatite during the hydrolytic dehydrogenation of ammonia-borane. Monitoring the hydrogen evolution from the catalytic hydrolysis of ammonia-borane provides an indirect route to follow the nucleation and autocatalytic surface growth of metal(0) nanoparticles from the reduction of a precatalyst in an aqueous medium.

Acknowledgements

Partial support by Turkish Academy of Sciences is gratefully acknowledged. MZ thanks to FABED for their partial support to his research.

Notes and references

[a] Department of Chemistry, Science Faculty, Yüzüncü Yil University, 65080, Van, Turkey; E-mail: zmehmet@yyu.edu.tr
[b] Department of Chemistry, Middle East Technical University, 06800, Ankara, Turkey;
[c] Department of Chemical Engineering and Applied Chemistry, Atilim University, 06836, Ankara, Turkey.

1 US Department of Energy (DOE), Basic Research Needs For the Hydrogen Economy, Report of the Basic Energy Sciences Workshop on Hydrogen Production, Storage and Use (http://science.energy.gov/~/media/bes/pdf/reports/files/nhe_rpt.pdf).
2 Lighting the Way Towards a Sustainable Energy Futures, Inter Academy Council (I.A.C.) Report Amsterdam, **2007**.
3 J. Turner, G. Sverdrup, K. Mann, P.G. Maness, B. Kroposki, M. Ghirardi, R.J. Evans and D. Blake, *Int. J. Energy Res*., 2008, **32**: 379.
4 Annual Energy Outlook 2005 With Projections To 2025, Energy Information Administration, February, 2005. (www.eia.doe.gov/oiaf/aeo/pdf/0383(2005).pdf)
5 S.H. Lim, J. Luo, Z. Zhong, W. Ji and J. Lin, *Inorg Chem* 2005, **44**, 4124.
6 J. Weitkamp, M. Fritz and S. Ernst, *Int J. Hydr. Energ.,* 1995, **20**, 967.
7 N.B. McKeown and P.M. Budd, *Chem. Soc. Rev.,* 2006, **35**, 675.

8 N.L. Rossi, J. Eckert, M. Eddaoudi, D.T. Vodak, J. Kim, M. O'Keefe and O.M. Yaghi, *Science* 2003, **300**, 1127.
9 M. Au and A. Jurgensen, *J. Phys. Chem. B.,* 2006, **110**, 7062.
10 M. Zahmakiran and S. Özkar, *Langmuir,* 2009, **25**, 2667.
11 E. Rönnebro and E.H. Majzoub, *J. Phys. Chem. B.*, 2007, **111**, 12045.
12 H.L. Jiang, S.K. Singh, J.M. Yan, X.B. Zhang and Q. Xu, *Chem Sus. Chem.*, 2010, **3**, 541.
13 A. Staubitz, A.P.M. Robertson and I. Manners, *Chem. Rev,.* 2010, **110**, 4079.
14 C.W. Yoon and L.G. Sneddon, *J. Am. Chem. Soc.,* 2006, **128**, 13992.
15 X. Huang, X. Chen, T. Yisgedu, E.A. Meyers, S.G. Shore and J. C. Zhao, *Inorg. Chem*., 2011, **50**, 3738.
16 S. Karahan and M. Zahmakiran and S. Özkar, *Int. J. Hyd. Energ.,* 2011, **36**, 4958.
17 C.W. Hamilton, R.T. Baker, A. Staubitz and I Manners, *Chem. Soc. Rev.* 2009, **38**, 279.
18 G. Wolf, J. Baumann, F. Baitalow and F.P. Hoffmann, *Thermochim. Acta*, 2000, **343**, 19.
19 C.A. Jaska, K. Temple, A.J. Lough and I. Manners, *J. Am. Chem. Soc.* 2003, **125**, 9424.
20 S. Çalışkan, M. Zahmakiran and S. Özkar, *App. Catal. B: Env.* 2010, **93**, 387.
21 H.L. Jiang and Q. Xu, *Catal. Tod.,* 2011, **170**, 56.
22 M. Zahmakiran, T. Ayvali, S. Akbayrak, S. Çalışkan, D. Çelik, S. Özkar, *Catal. Tod.* 2011, **170**, 76.
23 F.H. Stephens, V. Pons and R.T. Baker, *Dalton Trans.,* 2007, **25**, 2613.
24 M.E. Bluhm, M.G. Bradley, R. Butterick, U. Kusari and L.G. Sneddon, *J. Am. Chem. Soc.,* 2006, **128**, 7748.
25 A Web of Science literature search showed that in total > 120 studies exist according to the terms "catalytic hydrolysis of ammonia-borane". Please see recent excellent reviews given in references 12, 17, and 21, which briefly survey these catalysts systems.
26 H.Y. Liang, G.Z. Chen, Z. Desinan, R. Rosei, F. Roseiand D.L. Ma, Int. *J. Hydr. Energ.*, 2012, **37**, 1792.
27 S. Akbayrak and S. Özkar, *ACS App. Mater. Int.,* 2012, **4**, 6302.
28 H. Can and Ö. Metin, *App. Catal. B: Env.* 2012, **125**, 304.
29 M. Zahmakiran, *Mater. Sci. Eng. B.,* 2012, **177**, 606.
30 H.B. Dai, X.D. Kang and W. Ping, *Int. J. Hydr. Energ.,* 2010, **35**, 10317.
31 F. Durap, M. Zahmakiran and S. Özkar, *Int. J. Hydr. Energ.,* 2009, **34**, 7223.
32 Ö. Metin, Ş. Şahin and S. Özkar, *Int. J. Hydr. Energ*., 2009, **34**: 6304.
33 S. Basu, A. Brockman, P. Gagare, Y. Zheng, P.V. Ramachandran, W.N. Delgass and J.P. Gore, *J. Power Sources* 2009, **188**, 238.
34 J.C. Elliot, Structure and Chemistry of Apatites and Other Calcium Orthophosphates, Elsevier, Amsterdam, 1994.
35 K. Kaneda and T. Mizugaki, *Energ. Env. Sci.,* 2009, **2**, 655.
36 M. Zahmakiran, Y. Tonbul and S. Özkar, *Chem. Comm*., 2010, **46**, 4788.
37 M. Zahmakiran, Y. Román-Leshkov and Y. Zhang, *Langmuir,* 2012, **28**, 60.
38 S. Akbayrak, P. Erdek and S. Özkar, *App. Catal. B: Env.* 2013, **142-143**, 187.
39 Y. Tonbul, M. Zahmakiran and S. Özkar, *J. Am. Chem. Soc.,* 2010, **132**, 6541.
40 M.A. Watzky and R.G. Finke, *J. Am. Chem. Soc.,* 1997, **119**, 10382.
41 M. Zahmakiran and S. Özkar, *Inorg. Chem.,* 2009, **48**, 8955.
42 S. Çalışkan, M. Zahmakiran, F. Durap and S. Özkar, *Dalton Trans.,* 2012, **41**, 4976.
43 W.H. Press, B.P. Flannery, S.A. Teukolsky and W.T. Vetterling, Numerical Recipies, Cambridge University Press: Cambridge, UK, 1989.
44 D.W. Breck, Zeolite Molecular Sieves. Krieger: Malabal, FL, 1984.
45 J.A. Widegren, J.D. Aiken, S. Özkar and R.G. Finke, *Chem. Mater.,* 2001, **13**, 312.
46 J.A. Widegren, M.A. Bennett and R.G. Finke, *J. Am. Chem. Soc.,* 2003, **125**, 10301.
47 P.V. Ramachandran and P.D. Gagare, *Inorg. Chem.,* 2007, **46**, 7810.
48 Using the equation $N = N_o pV/101.07$, where $N_o = 6.022 \times 10^{23}$, p = 12.45 g cm^{-3} and $V = (4/3)\pi r^3$, the number of metal atoms in spherical 2.56 nm ruthenium(0) nanoclusters is estimated to be 147.
49 S. Storck, H. Bretinger and W.F. Maier, *App. Catal. A: Gen.,* 1998, **174**, 137.
50 C. Wagner, W.M. Riggs, L.E. Davis, J.F. Moulder and G.E. Muilenberg, Handbook of X-ray Photoelectron Spectroscopy, Perkin-Elmer, 1979.
51 Y. Lin and R.G. Finke, *J. Am. Chem. Soc.,* 1994, **116**, 8335.

Table of Content :

Nanohydroxyapatite supported ruthenium(0) nanoparticles formed in-situ during the hydrolysis of AB have been found to be highly active catalyst in the hydrogen generation from aqueous AB solution.